CILAMCE 2017
Florianópolis - Santa Catarina - Brazil

WIND RESOURCE ASSESSMENT USING OPENFOAM: A REAL TERRAIN CASE STUDY

William Correa Radunz

Adriane Prisco Petry

william.radunz@ufgrs.br

adrianep@mecanica.ufrgs.br

Department of Mechanical Engineering, Universidade Federal do Rio Grande do Sul

R. Sarmento Leite, 425, 90050-170, Rio Grande do Sul, Brazil

Abstract. *This paper presents a novel methodology for wind resource assessment in complex sites by employing the open-source C++ toolbox OpenFOAM. The framework consists in simulating the flow for at least twelve wind directions and applying a post-processing correction on the wind velocity field based on the measured wind data near Panambi. Subsequently, the wind maps are weighed by frequency of occurrence and overlapped into the overall wind power density map. A consistent combination of turbulence model, inflow conditions and wall-functions, which is able to produce a sustainable atmospheric surface layer, is achieved through the modification of standard wall-functions and the constants of the standard* $k-\epsilon$ *model. The assessed region demonstrated great potential for exploiting the wind resource, displaying wind power densities substantially enhanced due to the speed-up effect. Furthermore, it was possible to propose a layout strategy which maximized the power output whilst mitigating the likely effects of wake loss, although the latter has not been evaluated is the present work.*

Keywords: *Wind resource assessment, complex terrain, OpenFOAM*

1 INTRODUCTION

Wind Resource Assessment (WRA) is the quantification of wind resources to compute parameters such as mean wind speed, wind direction frequency rose and the average annual energy production (AEP) of a proposed wind farm. According to the Asian Development Bank (2014), "the bulk of the activities in this phase are wind measurement, AEP estimation based on wind flow modeling, computational fluid dynamics modeling for complex terrain, and estimation of loss and uncertainty."

Wind measurement campaigns consist in siting met masts equipped with anemometers, wind vanes, temperature, pressure and humidity sensors, and thereafter treating the obtained data to assess the potential for exploiting the wind resource. Despite the accuracy, met tower data are inherently limited to the vicinity of the tower. Under certain special conditions (e.g. plain terrain with few obstacles and no surface roughness change), it might be possible to extrapolate the measurements to the surroundings. In complex terrain, however, the atmospheric boundary layer (ABL) winds flow in a rather non-linear fashion, accelerating near the top of hills and rises and possibly displaying wake flow in the lee. The main objective of numerical wind flow simulation is to horizontally extrapolate the wind measurements obtaining a local wind map. The latter may be used for wind power plant layout optimization, namely micro-siting, and to estimate the AEP.

The two most common wind flow models found in literature are those based on the Jackson and Hunt (1975) linear approach and Computational Fluid Dynamics (CFD). The linear models, like WAsP (Wind Atlas Analysis and Application Program), tend to over-predict the speed-up effect since they assume attached flow and small terrain perturbations. In CFD, the Reynolds-Averaged Navier-Stokes (RANS) equations are solved by turbulence modeling, being theoretically superior at representing non-linear phenomena like flow separation and recirculation.

CFD models primarily solve the continuity and RANS equations where atmospheric stability effects like buoyancy are usually disregarded, therefore simulating a neutrally stratified atmosphere. Equilibrium inflow conditions are often assumed as well, leading to the classic Richards and Hoxey (1993) set of fully-developed profiles. Nonetheless, there is a intensively-discussed issue regarding the inconsistency between turbulence model, inflow conditions and wall-functions (WFs), which ultimately leads the assumed fully-developed profiles to change when the ought to remain homogeneous. This matter was solved by Balogh et al. (2012) through the use of atmospheric wall-functions based on the Richards and Hoxey (1993) inflow profiles. One of the advantages of OpenFOAM is that the former already has wall-functions implemented for wind flow, whilst most CFD packages use the classic sand-grain based wall-functions. Blocken et al. (2007) pointed out that these may be used for wind flow simulation as long as a correction to the small-scale roughness based on the aerodynamic roughness is made. However, this approach leads to restrictions regarding the first cell size at the wall and is code-dependent.

In this paper, the $k - \epsilon$ turbulence model is used in OpenFOAM to simulate the neutrally-stratified ASL flow over a real terrain in the region of Panambi. This C++ package is known for its state-of-the-art open-source code, which may be modified to suit any specific application. In particular for wind flow modeling, the main goal is to achieve coherence between turbulence model, wall-functions and inflow conditions. Therefore, a methodology capable of producing a data-based set of inflow conditions consistent with turbulence model and WF is employed. The consistent model is thereafter used to simulate wind fields from twelve directions, thus representing the complete aerodynamic behavior of the studied site. The wind maps are posteriorly corrected using the measured wind data, and, subsequently, weighed by frequency and overlapped to produce the overall wind power density map (WPDM).

The Launder and Spalding (1974) $k-\epsilon$ turbulence model, considerations about the consistency with the Richards and Hoxey (1993) boundary conditions and WFs, including proposed modifications are discussed in section 2. In section 3, the WRA methodology developed is presented, which includes the generation of boundary conditions based on the wind data and the post-processing field correction. Lastly, the weighed WPDMs are overlapped resulting in the overall WPDM. Results from the numerical simulation of a 2D empty fetch used for model verification and, ultimately, Panambi, are discussed in section 4. The main conclusions and insights of the paper are debated in section 5.

2 THEORY

According to Stull (2017), the ASL is the lowest portion of the ABL and it is where the surface effects of friction and heat convection have a major effect on the wind speed and temperature fields, which change substantially with height. One peculiarity of the ASL is that turbulent *momentum* and heat fluxes are somewhat uniform with height, which is why it is also known as constant flux layer. By neglecting the Coriolis (caused by the rotation of the Earth) and stratification effects, the lowest 200 m of the ABL can be modeled by the standard $k-\epsilon$ turbulence model, shown in index notation below

$$\nu_t = C_\mu \frac{k^2}{\epsilon} \tag{1}$$

$$\frac{\partial}{\partial x_i}(U_i k) = \frac{\partial}{\partial x_j}\left[\left(\nu + \frac{\nu_t}{\sigma_k}\right)\frac{\partial k}{\partial x_j}\right] + G_k - \epsilon \tag{2}$$

$$\frac{\partial}{\partial x_i}(U_i \epsilon) = \frac{\partial}{\partial x_j}\left[\left(\nu + \frac{\nu_t}{\sigma_\epsilon}\right)\frac{\partial \epsilon}{\partial x_j}\right] + C_{\epsilon 1} G_k \frac{\epsilon}{k} - C_{\epsilon 2}\frac{\epsilon^2}{k} \tag{3}$$

$$G_k = \nu_t \left(\frac{\partial U_i}{\partial x_j} + \frac{\partial U_j}{\partial x_i}\right)\frac{\partial U_i}{\partial x_j} \tag{4}$$

where ν_t is the turbulence kinematic viscosity, k is the turbulence kinetic energy (TKE) and ϵ its dissipation rate, U is the Reynolds-Averaged wind speed, ν is the kinematic viscosity of the air and G_k is the TKE production term. The standard model constants are the following:

$$C_{\epsilon 1} = 1.44, \quad C_{\epsilon 2} = 1.92, \quad C_\mu = 0.09, \quad \sigma_k = 1.0, \quad \sigma_\epsilon = 1.3 \tag{5}$$

These classic constants are usually modified for micro-scale atmospheric flow simulation since they were adjusted to engineering-scale flows. Richards and Norris (2011) elucidate that C_μ may be adjusted to fit the TKE in the atmosphere, but the turbulent Prandtl number of the dissipation rate also ought to be corrected in order to be consistent

$$C_\mu = \frac{u_\star^4}{k^2}, \quad \sigma_\epsilon = \frac{\kappa^2}{(C_{\epsilon 2} - C_{\epsilon 1})\sqrt{C_\mu}} \tag{6}$$

Richards and Hoxey (1993) proposed wind speed and turbulence profiles which produce homogeneous flow for the standard $k-\epsilon$ model. Under the assumptions of negligible vertical velocity, constant pressure and constant shear stress, the following set of inflow profiles are a solution to Eqs. (2) and (3)

$$u = \frac{u_\star}{\kappa} ln\left(\frac{z+z_0}{z_0}\right) \quad (7)$$

$$k = \frac{u_\star^2}{\sqrt{C_\mu}} \quad (8)$$

$$\epsilon = \frac{u_\star^3}{(z+z_0)} \quad (9)$$

The set of equations (7-9) has been extensively used in the fields of wind engineering and WRA. One of the most important implications that arise from the use of the aforementioned profiles is that they are a solution to the governing equations and, as such, are able to produce a fully-developed sustainable boundary layer. In micro-scale atmospheric modeling, the region of interest must be placed far away from the inlet in order to reduce the numerical error but, nonetheless, the wind profile immediately upstream the studied site should ideally present the same characteristics as the inflow conditions if the terrain is plain and uniformly covered by vegetation. When a combination of turbulence model, wall-functions and inflow conditions is said consistent, it is capable of sustaining a fully-developed boundary layer under the aforementioned conditions.

2.1 Ensuring model consistency

Even though these profiles should remain unchanged in the flow direction if the terrain is plain and there is no change in surface roughness, they might change due to an inconsistency between turbulence model, inflow conditions and WFs. In WRA and wind engineering, the ϵ and ν_t fields near the ground are usually treated by means of WFs. The problem, however, is that the value at the first cell-center near ground calculated by classic WFs based on the sand-grain roughness concept proposed by Nikuradse may not match the inflow profiles and, thus, cause flow inhomogeneity. It is possible, however, to modify the standard WFs and obtain model consistency similarly to authors Parente et al. (2011) and Balogh et al. (2012). The first method is to correlate the sand-grain roughness k_s to the atmospheric roughness length z_0, which is a code-dependent approach and imposes restrictions on the first cell height. A second alternative is to implement wall-functions which are consistent with the inflow conditions in such a fashion that the values calculated by the WFs are the same displayed by the incoming wind profile at that very node. In OpenFOAM, this is achieved by modifying *epsilonWallFunction* by adding z_0 to the following equations

$$\epsilon_P = \frac{C_\mu^{0.75} k^{1.5}}{\kappa(z_P)} \rightarrow \frac{C_\mu^{0.75} k^{1.5}}{\kappa(z_P+z_0)} \quad (10)$$

$$G_{k_P} = \frac{\tau_w^2}{\kappa C_\mu^{0.25} k_P^{0.5}(z_P)} \rightarrow \frac{\tau_w^2}{\kappa C_\mu^{0.25} k_P^{0.5}(z_P+z_0)} \quad (11)$$

where the subindex P stands for near-ground cell center. As for the ν_t WF, an atmospheric version compatible with the inflow conditions is already implemented, namely *nutkAtmRoughWallFunction*. Since a number of modifications have been made, it is necessary to assert that the model is indeed coherent with WFs and inflow conditions. Therefore, a model verification is performed in section 4, where wind flow is simulated in a bi-dimensional homogeneously-covered empty fetch.

3 METHODOLOGY

The WRA work-flow begins with the calculation of the master table containing the boundary condition parameters required for Eqs. (7-9) for each wind direction (twelve in this paper). The computational grid remains the same for all simulations for it allows field overlapping straightforwardly with reduced effort. To account for the different wind sectors, the boundary conditions rotate around the domain in 30° steps. Once all the simulations are run and the post-processing correction utility developed is applied, the overall WPDM is generated for Panambi.

3.1 Domain and boundary conditions

The analysis starts with the Digital Elevation Model (DEM) of the site and evaluation of the measured wind data, which is shown in Fig. 1. It can be observed that the topography of the region is complex and there is considerable spread in the wind frequency rose, which bolsters the importance of using CFD for WRA. Although the measured and treated data may not be fully disclosured due to confidentiality, a Python script has been developed for treating, grouping and calculating the inflow condition parameters and turbulence model constant. The procedure employs non-linear least squares to fit the annual mean wind speeds (AMWS) (which are available at 60, 80 and 100 m) with Eq. (7) and, thus, determining $u_\star$ and z_0. For the turbulence kinetic energy (TKE) profile, since Eq. (8) is constant with height, the curve fit is simply the mean value amongst measurements. From the latter, the turbulence model constant C_μ is obtained but limited to the maximum value of 1.0, as it may lead to convergence issues.

The computational domain consists of a kilometer-scale rectangular box with the terrain surface as its bottom. In CFD, one has input control over the boundary conditions only. Near the domain boundaries, the simulated fields are heavily biased and should not be regarded as reliable in any application, including WRA. Thus, the region of interest should be placed far away from the computational boundaries so that the error is reduced. In the present study, the site of interest consist of a 2 km x 2 km area around the met mast. This region must be limited as the uncertainties escalate quickly moving away from the tower, which is the reference site for applying the post-processing data correction. Therefore, the corrected wind speed values at the mast are exactly those measured and its vicinity is expected to represent the local wind climate more accurately than regions further away. The domain size is 10 km x 10 km x 1.5 km to allow the ASL to adapt to the orographic effects upstream and better represent the wind. Additionally, the height of the computational grid is exaggerated to mitigate the artificial blockage effect and the influence of the upper boundary conditions, and not because the ABL is being simulated to its full extent.

The inflow conditions used are those described by Eqs. (7-9) and represent a horizontally-homogeneous neutral ASL. The outlet patch was set as outflow. The slip condition is used when the wind direction vector is orthogonal (N, E, S and W), whilst for non-orthogonal directions the side patches are set either as inflow or outflow, as may be seen in Table 1. The ground

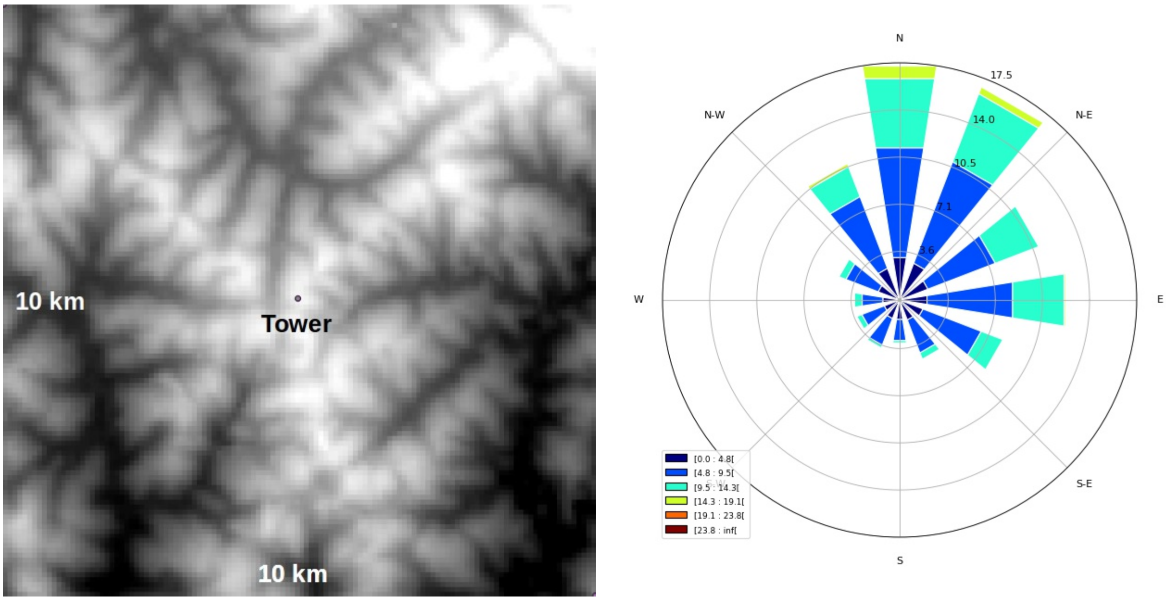

Figure 1: Digital Elevation Model of Panambi with the met mast found at the center (left) and frequency wind rose measured at the site (right).

of the terrain is modeled through the use of the fully-rough atmospheric wall-functions (described in section 2.1) with a uniform $z_0 = 0.1$ m since heterogeneous roughness has not been implemented in the methodology as of yet.

For the generation of the structured computational mesh, the utility *terrainBlockMesher* developed by Schimidt et al. (2012) was used. This application allows for splitting the domain in blocks with different grid densities so that more resolution is put into the region of interest. In addition, a very fine and smoothly-growing mesh is required in the lowest 200 m which represent the ASL. The final grid used for the WRA simulations of section 4.2 is shown in Fig. 2.

Table 1: Boundary condition types according to the wind direction

Wind Sector	0°	30-60°	90°	120-150°	180°	210-240°	270°	300-330°
North	*inlet*	*inlet*	*slip*	*outlet*	*outlet*	*outlet*	*slip*	*inlet*
East	*slip*	*inlet*	*inlet*	*inlet*	*slip*	*outlet*	*outlet*	*outlet*
South	*outlet*	*outlet*	*slip*	*inlet*	*inlet*	*inlet*	*slip*	*outlet*
West	*slip*	*outlet*	*outlet*	*outlet*	*slip*	*inlet*	*inlet*	*inlet*

3.2 Weighed field overlapping

The wind data is available exclusively at the anemometric tower and the purpose of the numerical simulation is to determine the micro-scale wind meteorology based on this data. Nonetheless, the wind conditions at the boundaries are not known beforehand and the model does not allow for information input other than at the boundaries. This situation can be overcome by using the wind speed and turbulence profiles at the met mast as input for the inflow

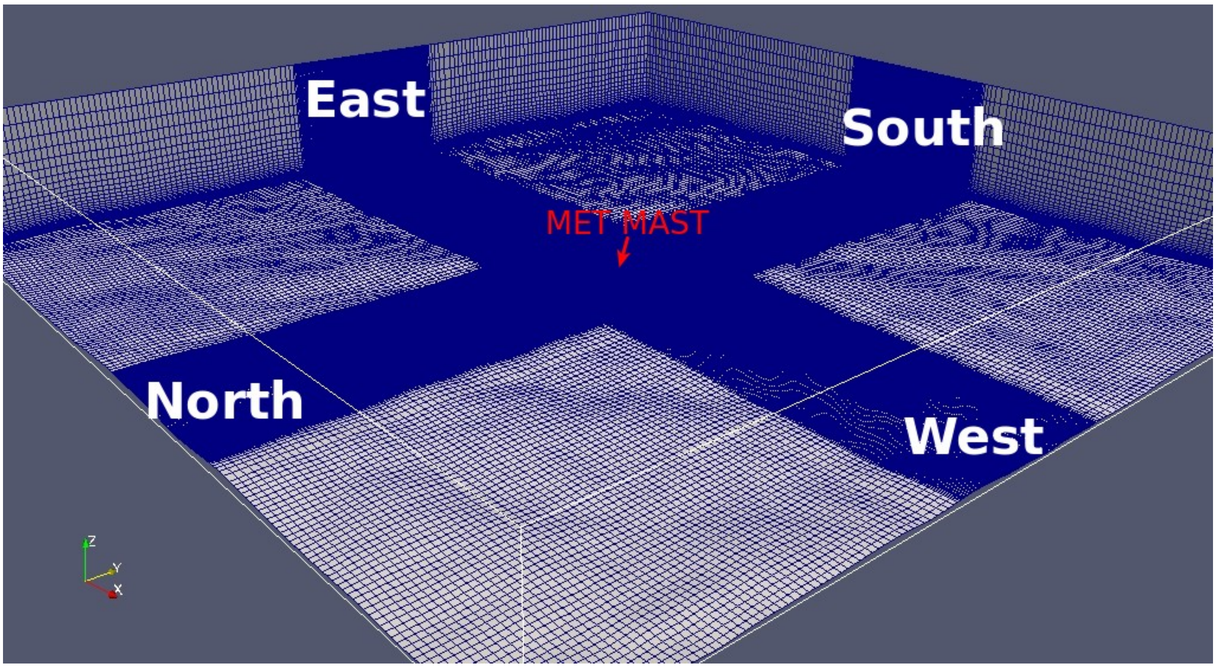

Figure 2: Computational grid "Fine" with 2,246,400 volumes. The finer central portion featured is the region of interest of this study.

conditions and construct a large domain, thus allowing the ASL to adjust to surface effects. In such scenario, the numerically simulated wind profile at the met mast will most likely differ from the measured data. This error is not acceptable at all in WRA, considering that the power output of wind turbines is proportional to the cube of wind speed, possibly rendering the wind farm project unfeasible.

Considering that the inflow conditions, WFs and turbulence model are consistent, the field is able to represent the relations between the wind speeds at different points of the domain, namely the wind speed-up (SU). The latter is a ratio between the wind speed at any point above ground level and that at the met tower

$$SU_i(x, y, z) = \frac{U_i(x, y, z)}{U_{i,t}(z)} \tag{12}$$

where U_i is the planar wind speed (since the vertical component is not measured by the cup anemometers and it has no contribution whatsoever to the power output of wind turbines) and $U_{i,t}$ is the simulated wind speed at the met mast and the subscript i denotes the wind direction. Hypothetically, the simulated SU field should be in better agreement with the real conditions, even if the the magnitude of the wind speeds are slightly offset. Subsequently, the correction to the CFD wind profile at the anemometer is employed and the corrected wind speed field $U_{i,corr}$ may be determined

$$CF_i(z) = \frac{U_{i,t,data}(z)}{U_{i,t}(z)} \tag{13}$$

$$U_{i,corr}(x, y, z) = CF_i(z)SU_i(z)U_{i,t}(x, y, z) \tag{14}$$

where CF_i is a height-dependent correction factor, $U_{i,t,data}$ is the measured wind profile and $U_{i,corr}$ is the corrected wind speed field. Afterwards, the wind power density is calculated for each wind sector through the following expression

$$P_i(x,y,z) = \frac{1}{2}\rho_i U_{corr}(x,y,z) \tag{15}$$

where P_i $[\mathrm{W\,m^{-2}}]$ is the wind power density, f_i the wind direction frequency and ρ_i $[\mathrm{kg\,m^{-3}}]$ the annual-mean air density. Ultimately, the overall annual-mean wind power density P $[\mathrm{W\,m^{-2}}]$ is given by the sum of the weighed power densities

$$P(x,y,z) = \sum_i^n f_i P_i(x,y,z) \tag{16}$$

The PDM has utmost importance for wind power plant layout optimization since it is the overlay of all directionally-dependent wind scenarios. Each simulated wind direction brings relevant information about the flow field at the site, although it is the sum of these conditions what truly represents the wind resource potential.

4 RESULTS AND DISCUSSION

The OpenFOAM solver *simpleFoam* was used for all the simulations in this section. It consists of a steady-state, incompressible, turbulent-flow solver which suits the modeling of the neutral ASL. The convection scheme was set as upwind for the U, k and ϵ fields. In what concerns the solvers, the Generalised Geometric-Algebraic Multi-Grid (GAMG) was used for pressure, whilst the Preconditioned Bi-Conjugate Gradient (PBiCG) was employed for the remaining fields. The solver convergence criteria was defined as 1E-4 for all fields with 0.3 relaxation factor for pressure and 0.7 for the remaining fields. All simulations were performed in parallel on four Intel Core i5-5200U @ 2.20GHz cores of a 6-GB-RAM laptop.

4.1 Empty fetch

A bi-dimensional empty fetch with 10 km along the flow direction and 1.5 km across was used to verify that the proposed model is indeed consistent and, thus, produces a horizontally-homogeneous ASL. The parameters used for the inflow conditions are those which represent the westerly wind with Eqs. (7-9). The consistent wall-functions were used for ϵ and ν_t fields, constant pressure outflow for p and inflow values specified at the top.

The results show that all profiles maintain their shape throughout the domain, as can be seen in Fig. 3. The U profile perfectly matches the inflow condition, although a small peak in the TKE is found near the ground. According to Richards and Norris (2011), this is not an inconsistency in the turbulence model, but rather a discretization issue with the TKE production term. Since this subtle phenomenon does not compromise the homogeneity of the ASL, the matter will have no further discussion.

4.2 Panambi

As a first step for the WRA simulations, it was necessary to evaluate the grid sensitivity and choose that which shows the best compromise between cost and accuracy. Four meshes were employed to simulate the arbitrarily-chosen westerly wind. In all cases, the surface grid cell height was fixed at 1 m and the maximum growth rate in the vertical direction at 1.2. The meshes parameters are shown in Table 2. The results of the simulations ran with the aforementioned

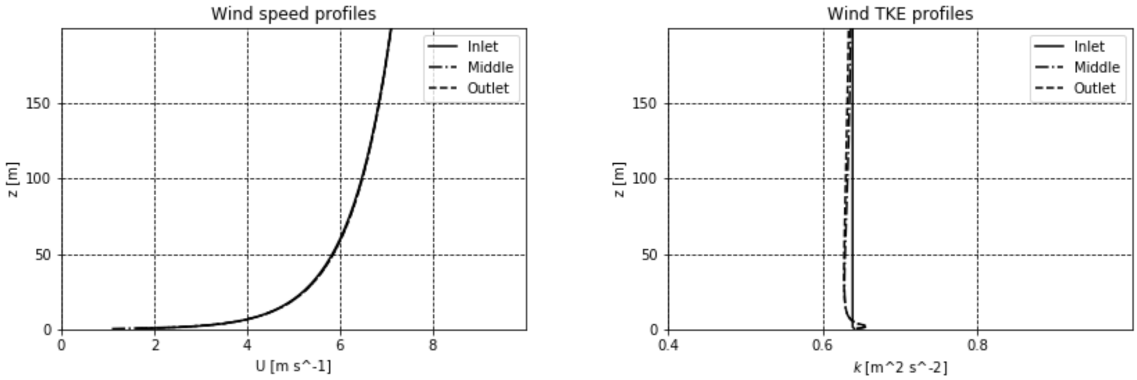

Figure 3: Wind speed (left) and TKE (right) profiles throughout the empty fetch domain.

grids show that the wind speed profiles at the met mast displayed little sensitivity to mesh refinement. Therefore, it was decided to evaluate the relative difference in wind speed between consecutive grids. It can be seen in Fig. 4 that the relative difference in wind speeds remains largely smaller than 0.2% between grids Fine-Finest and, thus, the Fine grid was chosen for the WRA.

Table 2: Grid parameters used for the sensitivity analysis

Grid	n_x	n_y	n_z	elements
Coarser	150	150	27	607,500
Coarse	180	180	32	1,036,800
Fine	240	240	39	2,246,400
Finest	270	270	53	3,863,700

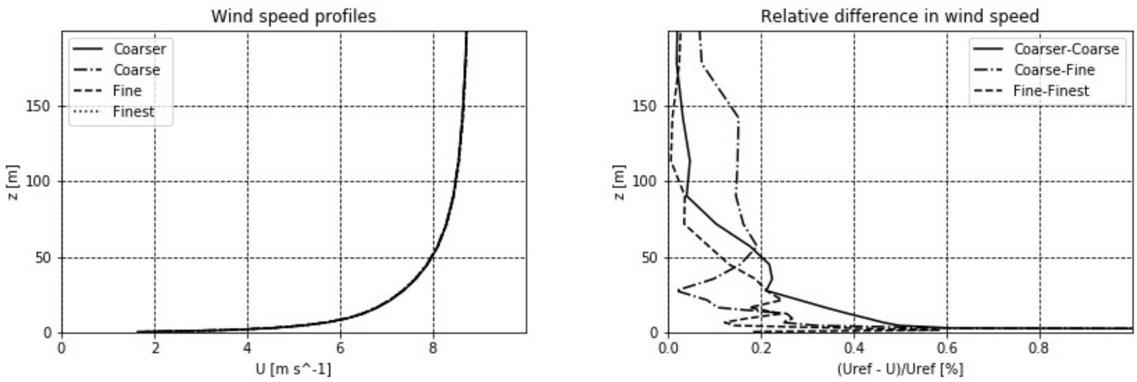

Figure 4: Wind speed profiles at the anemometer for the assessed grids (left). Relative difference between wind speed profiles of consecutive meshes (right).

The twelve WRA simulations were run in two grids so as to accelerate the convergence process. Firstly, each wind direction was simulated with the Coarser grid and the results were mapped into the Fine mesh for a final run. The first set of simulations have taken nearly 6 hours to converge and, once these results were mapped into the final grid, additional 12 hours were necessary to achieve full convergence.

The results shown in Fig. 5 suggest that the relative speed-up (SU) does change considerably with the simulated wind sector, which reinforces the idea that all wind direction must be taken into account for wind farm layout design. In addition, there can be observed a trend of the higher-SU areas being subtly aligned orthogonally to the incoming wind. This feature is rather welcome since wind turbines tend to be arranged in rows perpendicular to the main wind direction to mitigate wake loss.

The weighted PDMs 100 m above ground level, which are shown in Fig. 6, follow a pattern similar to the SU fields since wind power density is proportional to the third power of SU. It is important to point that the WPD is greater for some directions due to the higher frequency of occurrence of that direction, and not necessarily higher annual mean wind speeds. The maps display a power density field that varies substantially throughout the site and with the incoming wind direction. It may be observed that higher-power clusters tend to be elongated in a direction orthogonal to the incoming wind, which causes the optimum wind farm layout the be dependent on each direction. Therefore, it is necessary to evaluate their combined effect by means of a weighed-by-frequency superposition described in section 3.2, which is displayed in Fig. 7. Considering that the preferred wind direction for the site is NE, it is possible to take advantage of both the orography and wind conditions to optimize energy production. It is noticeable that the enhanced power density clusters still shown a chain-like behavior perpendicular to the preferred wind direction, which allows for placing the wind turbines at optimum locations whilst mitigating the wake effect. Also according to this map, WPD varies quite abruptly so that the power output could be reduced by over 50% just by moving tens of meters.

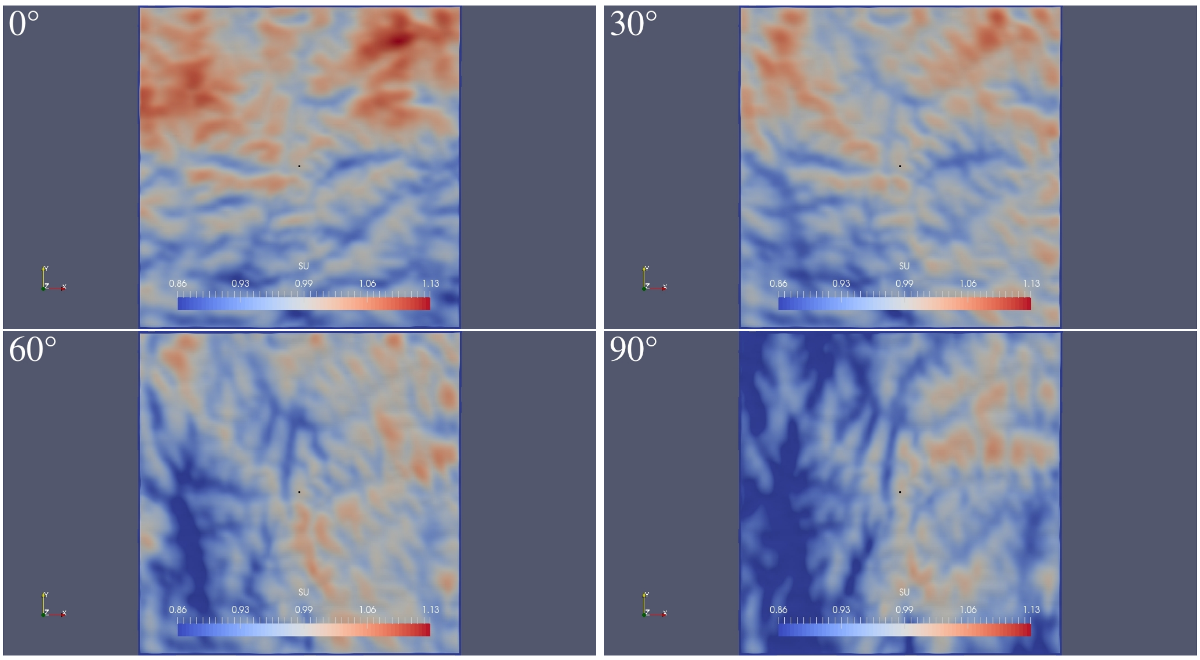

Figure 5: Simulated SU fields for wind directions 0° to 90° 100 m above ground level. The met mast is represented by the black dot at the center of the map.

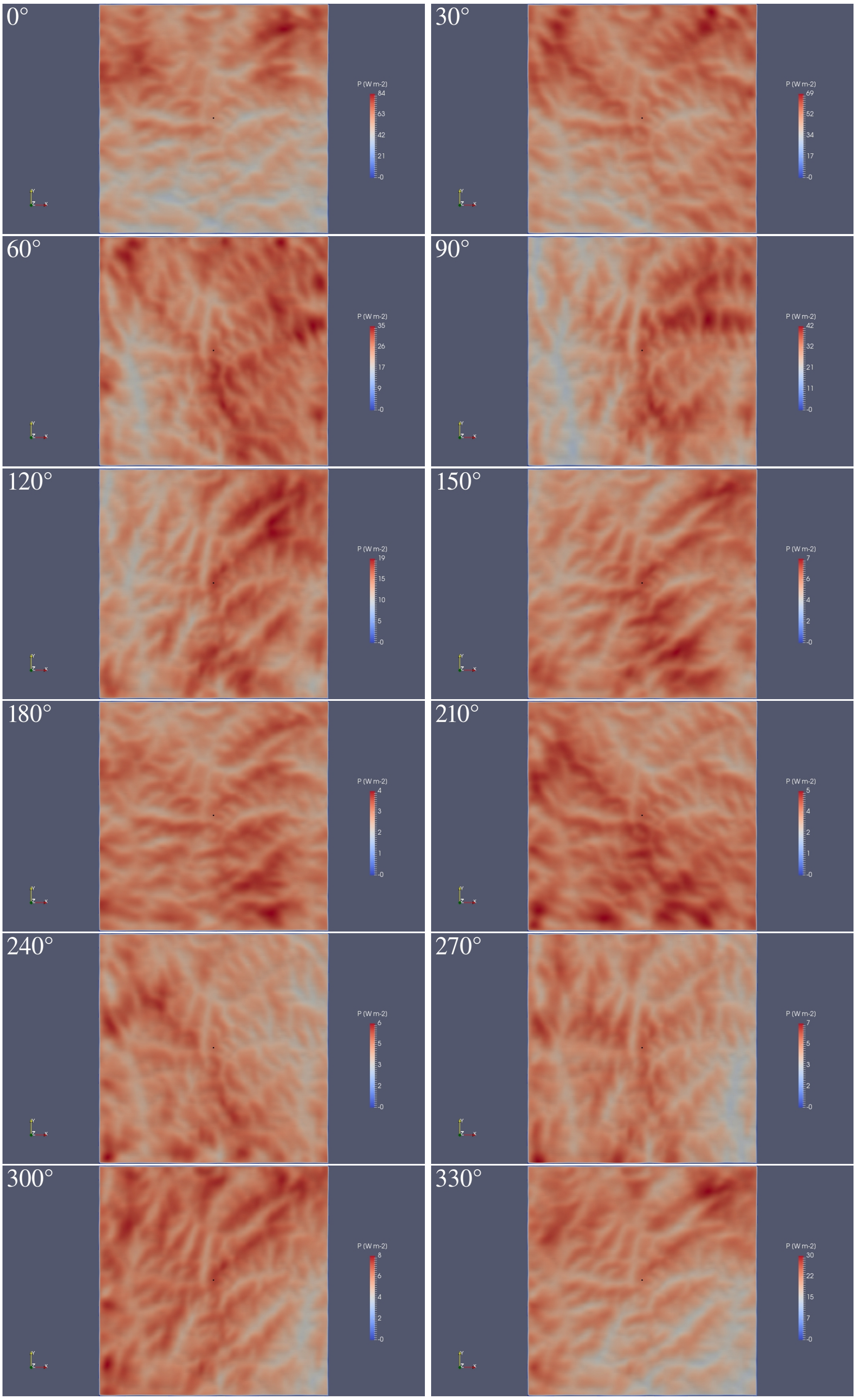

Figure 6: Simulated weighted WPDM for all wind directions 100 m above ground level. The met mast is represented by black dot at the center.

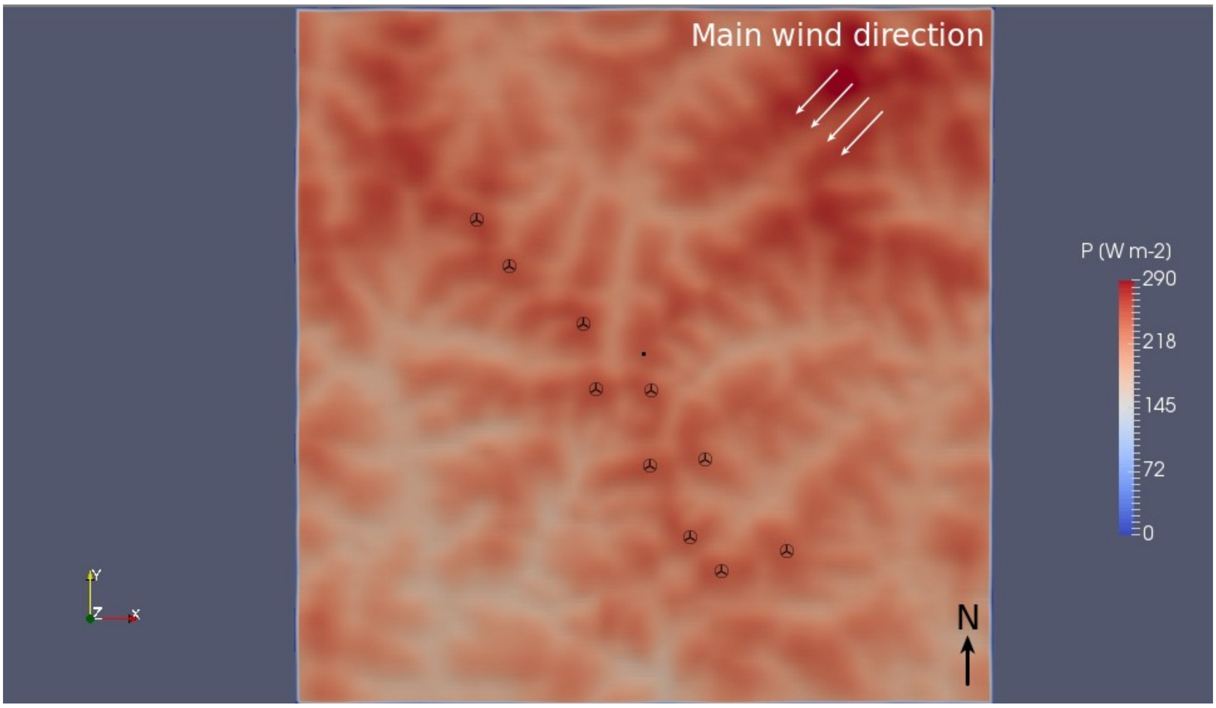

Figure 7: Overall WPDM for the Panambi region and the proposed micro-siting strategy. The wind turbine generators were orthogonally aligned to the main wind direction.

5 CONCLUSIONS

In this paper, a fully open-source methodology for WRA in complex terrain was implemented and used to evaluate the wind resource in the surroundings of Panambi. The OpenFOAM toolbox served as the main framework for simulating the neutrally-stratified ASL wind, which was done after ensuring that the turbulence model, wall-functions and inflow conditions were consistent – meaning they indeed generate a sustainable boundary layer.

One-year of measured wind data was used to generate boundary conditions for the CFD simulations and also to correct the wind fields as a post-processing utility. The work flow created was able to produce a detailed WPDM with modest processing resources and a reasonable time-frame. The region of Panambi features a significant potential for exploiting the wind resource mainly due to two reasons. Firstly, the wind power density near the top of some hills was found to be nearly twice the value in the surroundings which substantially increases the financial viability. Secondly, it was possible to propose a micro-siting layout in which the wind turbines are aligned orthogonally to the main wind direction whilst maximizing the energy production. This strategy is aimed at reducing the energy losses due to the upstream wind turbines wakes, although the modeling of the wakes is not approached in the present work.

Amongst the features to be approached in future works are the implementation of a stratification model, calculation of Weibull distribution maps, building a database with modern wind turbines to automatically estimate the annual energy production and implementation of a post-processing wake model. In addition, it is rather important to validate the methodology with wind farm data so that it may be used on new wind power plant projects with greater confidence.

ACKNOWLEDGEMENTS

The authors would like to thank the partnership and cooperation of the company Hidropan (Panambi, RS) in the project "Development of a Methodology for Wind Energy Assessment in Complex Terrain for Distributed Generation", which was jointly developed at the Federal University of Rio Grande do Sul (UFRGS) and inspired this work. The Brazilian National Council for Scientific and Technological Development (CNPq) and the Fluid Mechanics Laboratory (LMF - UFRGS) are also highly regarded for their contributions.

REFERENCES

Balogh, M., Parente, A., & Benocci, C., 2012. RANS simulation of ABL flow over complex terrains applying an Enhanced $k-\epsilon$ model and wall function formulation: Implementation and comparison for fluent and OpenFOAM. *Journal of Wind Engineering and Industrial Aerodynamics*, vol. 104-106, pp. 360-368.

Blocken, B., Stathopoulos, T., & Carmeliet, J., 2007. CFD simulation of the atmospheric boundary layer: wall function problems. *Atmospheric Environment*, vol. 41, pp. 238-252.

Jackson, P. S., & Hunt, J. C. R., 1975. Turbulent windflow over a low hill. *Quarterly Journal of the Royal Meteorology Society*, vol. 101, pp. 929-955.

Launder, B. E., & Spalding, D. B., 1974. The numerical computation of turbulent flows. *Computer Methods in Applied Mechanics and Engineering*, vol. 3, pp. 269-289.

Parente, A., Gorl, C., van Beeck, J., & Benocci, C., 2011. Improved $k-\epsilon$ model and wall function formulation for the RANS simulation of ABL flows. *Journal of Wind Engineering and Industrial Aerodynamics*, vol. 99, pp 267-278.

Richards, P. J., & Hoxey, R., 1993. Appropriate boundary conditions for computational wind engineering models using the $k-\epsilon$ turbulence model. *Journal of Wind Engineering and Industrial Aerodynamics*, vol. 47, pp 145-153.

Richards, P. J., & Norris, S. E., 2011. Appropriate boundary conditions for computational wind engineering models revisited. *Journal of Wind Engineering and Industrial Aerodynamics*, vol. 99, pp 257-266.

Schmidt, J., Peralta, C., & Stoevesandt, B., 2012. Automated Generation of Structured Meshes for Wind Energy Applications. *Open Source CFD International Conference*.

Stull, R., 2017. Practical Meteorology: An Algebra-based Survey of Atmospheric Science. University of British Columbia. 938 p.

Zhang, M. H., 2015. Wind Resource Assessment and Micro-Siting: Science and Engineering. 1st ed. Singapore: Wiley. 293 p.